A&A 514, A26 (2010)
DOI: 10.1051/0004-6361/200913218

Astronomy & Astrophysics

Reconnection in weakly stochastic *B*-fields in 2D

K. Kulpa-Dybeł[1], G. Kowal[1,2], K. Otmianowska-Mazur[1], A. Lazarian[2], and E. Vishniac[3]

[1] Astronomical Observatory, Jagiellonian University, ul Orla 171, 30-244 Kraków, Poland
e-mail: kulpa@oa.uj.edu.pl
[2] Department of Astronomy, University of Wisconsin, 475 North Charter Street, Madison, WI 53706, USA
[3] Department of Physics and Astronomy, McMaster University, 1280 Main Street West, Hamilton, ON L8S 4M1, Canada

Received 31 August 2009 / Accepted 5 January 2010

ABSTRACT

We study two-dimensional turbulent magnetic reconnection in a compressible fluid in the gas pressure dominated limit. We use open boundary conditions and start from a Harris current sheet configuration with a uniform total pressure. A small perturbation of the vector potential initiates laminar reconnection at the Sweet-Parker rate, which is allowed to evolve for several dynamical times. Subsequently sub-Alfvenic turbulence is produced through random forcing at small wave numbers. The magnetic field topology near the current sheet is strongly affected by the turbulence. However, we find that the resulting reconnection speed depends on the resistivity. In contrast to previous results in three dimensions, we find no evidence for fast reconnection. The reconnection speed exhibits strong variations, but the time averages increase smoothly with the strength of the turbulence.

Key words. galaxies: magnetic fields – turbulence – magnetohydrodynamics (MHD)

1. Introduction

Radio observations of a wide variety of astrophysical bodies (the Sun, spiral galaxies, the Earth) show that a magnetic field is usually present (see Priest & Forbes 2000, for review). These magnetic fields have significant large scale components, i.e on the scale of the objects themselves. The origin of these fields is typically ascribed to the operation of a large scale magnetohydrodynamic dynamo (Ruzmaikin et al. 1988; Parker 1979, 1992; Hanasz et al. 2004; Lazarian & Vishniac 2008). Since dynamo theory involves the twisting and folding of field lines, it is important that there is some process which can lead to efficient smoothing of the small scale components of the field. In other words, we need to invoke some kind of fast local magnetic diffusion. Even though astrophysical fluids are turbulent (see Armstrong et al. 1995; Horbury & Balogh 2001; Elmegreen & Scalo 2004; McKee & Ostriker 2007), the concept of turbulent magnetic diffusivity (see Blackman & Field 2008), a popular heuristic concept used in early dynamo work, is known to be ill-founded (Cattaneo & Vainshtein 1991; Gruzinov & Diamond 1994; Vainshtein & Cattaneo 1992). In particular, it does not address the key question of how intersecting magnetic fluxes can change their topology. In an ionized plasma, Ohmic diffusivity fails by many orders of magnitude to supply the required magnetic diffusion.

For astrophysical dynamos to function smoothly, there must be a process which allows reconnection to proceed at speeds characteristic of local dynamical velocities. Since rms fluid velocities are often comparable to the local Alfvén speed, this requirement is in practice indistinguishable from $V_{\rm rec} \sim V_{\rm A}$. This is called fast reconnection, meaning that it does not depend on resistivity or depends on the resistivity logarithmically (see Parker 1979). There is also direct evidence for fast reconnection from studies of solar flares (Yokoyama & Shibata 1995; Innes et al. 1997; Pagano et al. 2008).

The idea that there could be some way of producing fast magnetic reconnection even in highly conducting fluids is not new (Moffat 1978; Krause & Radler 1980), but early models of reconnection (e.g. see Parker 1957; Sweet 1958) using realistic astrophysical temperatures and densities gave a very slow reconnection rate, $\sim V_{\rm A} S^{-1/2}$, where $S \equiv \eta/(V_{\rm A} L)$ is the Lundquist number, η is the resistivity, and L is the size of the current sheet. It was Petschek (1964) who for the first time introduced a model for fast reconnection with a rate proportional to $(\log S)^{-1}$. Subsequent numerical simulations and theoretical analyses have shown that the Petschek reconnection rate is only attainable in very restricted circumstances. For instance, a modified version can stably persist in a collisionless plasma (e.g. see Drake et al. 2006). This means that the length of the current sheet should not exceed approximately 50 electron mean free paths (Uzdensky 2006; Yamada et al. 2006). This condition cannot be satisfied in many astrophysical environments, e.g. in the interstellar medium (Vishniac & Lazarian 1999). In a collisional plasma the X-point region required for Petschek reconnection will collapse to the Sweet-Parker geometry for large S (Biskamp 1996).

The failure of the Petschek model has increased interest in the role of turbulence in reconnection. This interest has been further stimulated because the turbulence is ubiquitous in astrophysical environments where reconnection occurs, e.g. the ISM, stars, the Sun and accretion disks (Ruzmaikin et al. 1988). The idea that turbulence can affect reconnection has a long history, although it was usually studied in two-dimensions (2D) (Priest & Forbes 2000). Several researchers have approached this problem numerically, e.g. Matthaeus & Lamkin (1985, 1986); Fan et al. (2004, 2005); Servidio et al. (2009); Loureiro et al. (2009). They found that it was possible to get many features expected from reconnection theory, i.e. large and small-scale magnetic islands, fluid jetting, and current filamentation and that the maximum reconnection speed was higher for more powerful turbulence and exceeded the Sweet-Parker rate (Fan et al. 2004, 2005).

The most interesting result of their calculations (Fan et al. 2004, 2005) was that under the influence of turbulence they observed a two-step process of magnetic reconnection: beginning with a slow Sweet-Parker mechanism and changing later to a faster reconnection state that they identified with the Petscheck process. In a similar manner, the most recent paper (Loureiro et al. 2009) also observed that the presence of turbulence significantly enhances the reconnection rate. They further found that for a given value of diffusion and above a critical value of the turbulent injection power the reconnection process accelerates substantially. However, in all these simulations the authors used periodic boundary conditions, which prevents inflow or outflow and conserves the total magnetic flux. This made the actual reconnection rates difficult to evaluate. In particular, it was impossible to calculate the average reconnection rate, which is important in view of the large fluctuations induced by turbulence. In addition, one can argue that the reconnection rate in these simulations is influenced by the conservation of the total magnetic helicity (Blackman 2000). These difficulties can be avoided by using boundary conditions that allow the inflow and outflow of plasma and magnetic flux (Kowal et al. 2009).

More recently interest in the magnetic reconnection process has moved from 2D magnetic configurations to more realistic and generic three-dimensional ones. In particular, Lazarian & Vishniac (1999, LV99) and Lazarian & Vishniac (2000) proposed that in three dimensions a stochastic magnetic field component can dramatically enhance reconnection rates, leading to reconnection speeds comparable to the local turbulent velocity. Their model is based on the Sweet-Parker reconnection scheme, with a long narrow current sheet between two regions of dramatically different polarizations but similarly strong magnetic fields, but it also includes the effects of turbulence and substructure in the magnetic field. This has two principal effects. First, in three dimensions many independent patches of magnetic field come into contact with the current sheet and undergo reconnection. Second, the outflow of plasma and shared magnetic flux happens not over a microscopically narrow region determined by Ohmic diffusion, but through a substantially wider region determined by field wandering. Neither effect is present in two-dimensions, although the formation of magnetic islands in two-dimensions is roughly similar to the broadening of the outflow. Together these effects are sufficient to trigger fast magnetic reconnection. In this model the reconnection rate does not depend on the Ohmic resistivity, but is determined only by turbulence, in particular by its strength and injection scale. This fast reconnection model has been tested numerically by Kowal et al. (2009) using inflow/outflow boundary conditions and a wide range of injection scales and power for the turbulence. These simulations have confirmed all of the predicted features of the LV99 model, including the insensitivity to the Lundquist number.

In this paper we return to two-dimensional reconnection using the same inflow/outflow boundary conditions. We have two objectives in this work. First, since the explanation for fast reconnection advanced in LV99 was intrinsically three dimensional, we are interested in examining the effects of dimensionality on the reconnection rate. Second, this work constitutes an examination of the importance of boundary conditions on the two-dimensional model and a test of claims for fast reconnection in two-dimensions. Our numerical model of turbulent reconnection in the ISM is calculated in a 2D box with open boundary conditions. We use a Harris current sheet setup as an initial configuration. Reconnection develops as a result of an initial vector potential perturbation. We do not drive reconnection. We solve 2D non-ideal normalized isothermal MHD equations numerically while varying the power and scale of turbulence, and the magnetic resistivity (Kowal et al. 2009).

The plan of this paper is as follows. In Sect. 2 we describe the numerical setup and input parameters, and we present our method to measure the reconnection rate. The results are discussed in Sect. 3, where we analyze the time evolution of models with different power of injecting turbulence. We present the dependencies of the reconnection rate on the power of turbulence, the injection scale, the viscosity and uniform and anomalous resistivities. We also check the influence of initial magnetic field configuration, boundary conditions and the method of driving turbulence. We discuss our results in Sect. 4 and give our conclusions in Sect. 5.

2. Methods

2.1. Basic equations

We studied the problem of magnetic reconnection in the presence of weak turbulence using the magnetized fluid approximation governed by the isothermal non-ideal MHD equations of the form

$$\frac{\partial \rho}{\partial t} + \nabla \cdot (\rho \boldsymbol{v}) = 0, \tag{1}$$

$$\frac{\partial \rho \boldsymbol{v}}{\partial t} + \nabla \cdot (\rho \boldsymbol{v}\boldsymbol{v} + P_* \boldsymbol{I} - \boldsymbol{B}\boldsymbol{B}) = \boldsymbol{f} + \nu \Delta \boldsymbol{v}, \tag{2}$$

$$\frac{\partial \boldsymbol{A}}{\partial t} = \boldsymbol{v} \times \boldsymbol{B} - \eta \nabla \times \boldsymbol{B}, \tag{3}$$

where ρ is the gas density, $\boldsymbol{v}$ is the fluid velocity, $\boldsymbol{A}$ is the magnetic vector potential, $\boldsymbol{B} \equiv \nabla \times \boldsymbol{A}$ is the magnetic field, $P_* = c_s^2 \rho + B^2/8\pi$ is the total pressure, $\boldsymbol{I}$ is the Kronecker delta, c_s is the isothermal speed of sound, η is the resistivity coefficient, ν is the viscosity, $\boldsymbol{f} = \rho \boldsymbol{a}$ represents the forcing term, and $\boldsymbol{a}$ is a random acceleration.

We solved the MHD equations using the same code as in Kowal et al. (2009) based on the following methods: a higher-order shock-capturing Godunov-type scheme, the essentially non-oscillatory (ENO) spatial reconstruction (e.g. see Londrillo & Del Zanna (2000); Del Zanna et al. (2003)), a multi-state Harten-Lax-van Leer (HLLD) approximate Riemann solver for isothermal MHD equations (Mignone 2007) and the Runge-Kutta (RK) time integration (e.g. see Del Zanna et al. 2003). The choice of HLLD Riemann solver guarantees a good solution for the Alfvén wave propagation, which is important in our model, since most of the kinetic energy is transported through Alfvén waves (see Kowal et al. 2009). The divergence of the magnetic field must be kept zero everywhere at all times ($\nabla \cdot \boldsymbol{B} = 0$). To satisfy this condition the field interpolated constraint transport (CT) scheme based on the staggered grid is used (e.g. see Londrillo & Del Zanna 2000).

Some selected simulations that we performed include anomalous resistivity modeled as

$$\eta = \eta_u + \eta_a \left(\frac{|\boldsymbol{j}|}{j_{crit}} - 1 \right) H \left(\frac{|\boldsymbol{j}|}{j_{crit}} \right), \tag{4}$$

where η_u and η_a describe uniform and anomalous resistivity coefficients, respectively, j_{crit} is the critical level of the absolute value of current density above which the anomalous effects start to work, and H is a step function. However, for most of our simulations $\eta_a = 0$.

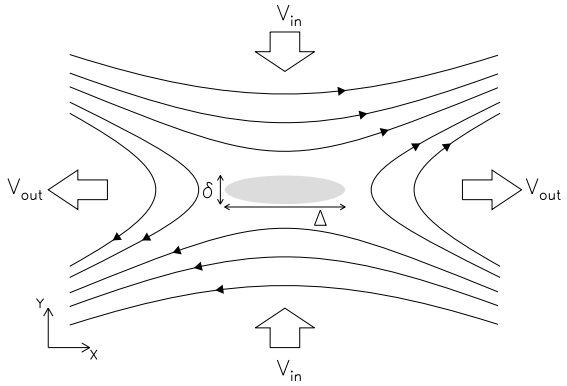

Fig. 1. 2D magnetic field configuration in our problem. The grey area describes the diffusion region where the incoming field lines reconnect. The longitudinal and transverse scales of the diffusion region are described by the parameters Δ and δ, respectively. We use inflow and outflow boundary conditions at X and Y directions, respectively.

2.2. Initial and boundary conditions

We numerically investigated the turbulent magnetic reconnection model in 2D in a computational box of the size $L_x \times L_y$, where $L_x = 1$ and $L_y = 2$ with a spatial resolution of 1024×2048 grid zones in the x and y directions, respectively. Figure 1 shows a 2D visualization of the reconnection problem setup. The domain contains two regions of oppositely directed magnetic lines separated by a diffusion region with a thickness δ and a length Δ, where the magnetic lines reconnect and the product of this process is ejected along the X direction with a speed $V_{\rm out}$ (see Fig. 1). The initial magnetic field configuration is described by a Harris current sheet $B_x(x, y) = B_{x0} \tanh(y/\theta)$, where B_{x0} is the initial strength of the anti-parallel magnetic field component and θ is the initial thickness of the current sheet. The Sweet-Parker reconnection is triggered by a small initial perturbation of the vector potential $\delta \boldsymbol{A}(x, y) = \delta B_0 \cos(2\pi x) \exp[-(y/d)^2]$, where d and δB_0 denote the thickness of the perturbed region and the strength of the initial perturbation, respectively. The initial setup is completed by setting the density profile from the condition of the uniform total pressure $P_*(t = 0, x, y) = \text{const.}$ and setting the initial velocity to zero everywhere.

The code (Kowal et al. 2009) uses dimensionless units. The velocity and magnetic field are expressed in units of the characteristic Alfvén speed $V_{\rm A} \equiv |B_{x0}|/\sqrt{\rho_0}$, where the initial anti-parallel component of magnetic field $B_{x0} = 1$ and the density $\rho_0 = 1$ far from the diffusion region so that $V_{\rm A} = 1$ far from the diffusion region in all models. Time is measured in units of the Alfvén transit time $t_{\rm A} \equiv 1/V_{\rm A}$. In all models we used the same value of the initial thickness of the current sheet $\theta = 0.05$. The speed of sound was set to $c_{\rm s} = 4$ (the plasma $\beta \equiv p/p_{\rm mag}$ was 32.0 for all models). We varied the resistivity coefficient $\eta_{\rm u}$ between values 3×10^{-4} and 5×10^{-3} (in dimensionless units). In the models which include anomalous effects, we varied the anomalous resistivity coefficient $\eta_{\rm a}$ between 0.0 and 3×10^{-3}. The parameters describing the initial perturbation were set to $\delta B_0 = 0.05$ and $d = 0.1$.

We used outflow boundary conditions along the X direction and inflow boundary conditions along the Y direction, setting the normal derivatives of the fluid variables (density and momentum) to zero. In the treatment of vector potential $\boldsymbol{A}$ at the boundary we set its components transverse to the considered boundary using the first order extrapolation, while the normal derivative of the normal component was set to zero. This guaranteed that all waves generated in the system were free to leave the box without significant reflections. For a more detailed description of these boundary conditions including their advantages and drawbacks we refer the reader to Kowal et al. (2009).

2.3. Model of turbulence

In order to drive turbulence in our model we followed Kowal et al. (2009) and used the method proposed by Alvelius (1999). The forcing was driven across a specified distribution of wave vectors. Here we used a Gaussian profile around a shell in Fourier space with a radius which determined the injection scale $l_{\rm inj}$. The forcing was random in time and it was therefore uncorrelated with any of the time scales of the turbulent flow. For the same reason the power input was defined purely by the force-velocity correlation. The driving was completely solenoidal and did not directly produce density fluctuations.

Forcing was imposed in the vicinity of the midplane, namely in the region between $y = -0.25$ and $y = 0.25$. Turbulence was introduced at a given injection scale and grew gradually in time until it reached the desired amplitude corresponding to the turbulent power $P_{\rm inj}$. We drove the turbulence to its saturation level over one Alfvénic time from $t_{\rm beg} = 9$ to $t_{\rm end} = 10$. According to the LV99 model, the injection scale and turbulent power determine the rate of reconnection in 3D. Thus, in our model we tested this correlation in 2D by changing these properties of turbulence.

2.4. Input parameters

Our simulations can be divided into five groups. In each of them we analyze the dependence of the reconnection rate by changing only one of the crucial parameters: for models PD – the power of turbulence $P_{\rm inj}$, for models SD – the injection wavenumber $k_{\rm f}$, for models VD – viscosity ν, for models RD and AD the uniform $\eta_{\rm u}$ and anomalous $\eta_{\rm a}$ resistivities, respectively. In Table 1 we list parameters of all the models presented in this paper.

Among all parameters of the model we list those which vary, i.e. the uniform and anomalous resistivities, $\eta_{\rm u}$ and $\eta_{\rm a}$, respectively, the uniform viscosity ν, the power of turbulence $P_{\rm inj}$ and its injection wavenumber $k_{\rm inj}$ with the half-thickness of the injection shell $\Delta k_{\rm inj}$, the number of perturbed Fourier components of velocity $N_{\rm f}$ and the amplitude of perturbation $\tilde{v}_{\rm f}$ at the injection scale. In addition, we include the mean velocity amplitude obtained at the end of each simulation.

2.5. Reconnection rate measure

For the laminar reconnection (Sweet-Parker and Petschek) the rate can be measured by averaging the inflow velocity $V_{\rm in}$ divided by the Alfvén speed $V_{\rm A}$ over the inflow boundaries, i.e.

$$\langle V_{\rm in}/V_{\rm A}\rangle = \frac{1}{2}\int_{x_{\rm min}}^{x_{\rm max}} {\rm d}x \left(\frac{v_y}{V_{\rm A}}\bigg|_{y=y_{\rm min}} - \frac{v_y}{V_{\rm A}}\bigg|_{y=y_{\rm max}} \right). \quad (5)$$

Since we had two X boundaries, located at $y = y_{\rm min}$ and $y = y_{\rm max}$, we needed to take half of the resulting integral. This measure works well for laminar reconnection, when the system is perfectly stable and where the time derivative of the magnetic flux is zero. In the presence of turbulence, however, this time derivative can fluctuate or the turbulence in the center of the box can affect the flow of the plasma. In this way we would get a flow of magnetic flux without the presence of reconnection. To include all effects that contribute to the change of the magnetic flux, we

Table 1. List of models.

Name	η_u [10^{-3}]	η_a [10^{-3}	ν [10^{-3}]	P_{inj}	k_{inj}	Δk_{inj}	N_f	$\tilde{v}_f$	$\langle \lvert \boldsymbol{v} \rvert \rangle$
PD	0.5	0.0	0.0	0.005	12	0.5	68	0.00006	0.03983
	0.5	0.0	0.0	0.01	12	0.5	68	0.00009	0.04912
	0.5	0.0	0.0	0.05	12	0.5	68	0.00019	0.08401
	0.5	0.0	0.0	0.1	12	0.5	68	0.00028	0.10645
	0.5	0.0	0.0	0.5	12	0.5	68	0.00062	0.21685
	0.5	0.0	0.0	1.0	12	0.5	68	0.00088	0.28657
SD	0.5	0.0	0.0	0.1	8	0.5	48	0.00033	0.11618
	0.5	0.0	0.0	0.1	12	0.5	68	0.00028	0.10645
	0.5	0.0	0.0	0.1	16	0.5	112	0.00029	0.08927
	0.5	0.0	0.0	0.1	20	0.5	112	0.00023	0.06626
	0.5	0.0	0.0	0.1	24	1.0	36	0.00042	0.05534
	0.5	0.0	0.0	0.1	28	1.0	32	0.00058	0.04633
	0.5	0.0	0.0	0.1	32	1.0	32	0.00056	0.03997
RD	0.3	0.0	0.0	0.01	12	1.0	68	0.00009	0.05734
	0.5	0.0	0.0	0.01	12	1.0	68	0.00009	0.04912
	0.6	0.0	0.0	0.01	12	1.0	68	0.00009	0.04471
	0.7	0.0	0.0	0.01	12	1.0	68	0.00009	0.04889
	0.8	0.0	0.0	0.01	12	1.0	68	0.00009	0.05405
	0.9	0.0	0.0	0.01	12	1.0	68	0.00009	0.04813
	1.0	0.0	0.0	0.01	12	1.0	68	0.00009	0.05481
	2.0	0.0	0.0	0.01	12	1.0	68	0.00009	0.05542
	3.0	0.0	0.0	0.01	12	1.0	68	0.00009	0.06214
	4.0	0.0	0.0	0.01	12	1.0	68	0.00009	0.06774
	5.0	0.0	0.0	0.01	12	1.0	68	0.00009	0.07407
	0.3	0.0	0.0	0.1	12	1.0	68	0.00028	0.11583
	0.5	0.0	0.0	0.1	12	1.0	68	0.00028	0.10649
	0.6	0.0	0.0	0.1	12	1.0	68	0.00028	0.10763
	0.7	0.0	0.0	0.1	12	1.0	68	0.00028	0.10122
	0.8	0.0	0.0	0.1	12	1.0	68	0.00028	0.10221
	0.9	0.0	0.0	0.1	12	1.0	68	0.00028	0.10036
	1.0	0.0	0.0	0.1	12	1.0	68	0.00028	0.09854
	2.0	0.0	0.0	0.1	12	1.0	68	0.00028	0.08844
	3.0	0.0	0.0	0.1	12	1.0	68	0.00028	0.08075
	4.0	0.0	0.0	0.1	12	1.0	68	0.00028	0.07236
	5.0	0.0	0.0	0.1	12	1.0	68	0.00028	0.06987
AD	0.5	0.0	0.0	0.1	12	1.0	68	0.00028	0.10645
	0.5	0.5	0.0	0.1	12	1.0	68	0.00028	0.10534
	0.5	1.0	0.0	0.1	12	1.0	68	0.00028	0.11071
	0.5	2.0	0.0	0.1	12	1.0	68	0.00028	0.11252
	0.5	3.0	0.0	0.1	12	1.0	68	0.00028	0.11465
VD	0.5	0.0	0.08	0.1	12	1.0	68	0.00028	0.10372
	0.5	0.0	0.09	0.1	12	1.0	68	0.00028	0.09623
	0.5	0.0	0.10	0.1	12	1.0	68	0.00028	0.09041
	0.5	0.0	0.20	0.1	12	1.0	68	0.00028	0.08472
	0.5	0.0	0.30	0.1	12	1.0	68	0.00028	0.08366
	0.5	0.0	0.50	0.1	12	1.0	68	0.00028	0.07317
	0.5	0.0	0.60	0.1	12	1.0	68	0.00028	0.06957
	0.5	0.0	0.80	0.1	12	1.0	68	0.00028	0.06868
	0.5	0.0	1.00	0.1	12	1.0	68	0.00028	0.06019
	0.5	0.0	2.00	0.1	12	1.0	68	0.00028	0.04371
	0.5	0.0	3.00	0.1	12	1.0	68	0.00028	0.03852
	0.5	0.0	4.00	0.1	12	1.0	68	0.00028	0.03394
	0.5	0.0	5.00	0.1	12	1.0	68	0.00028	0.02912

used a new and more general measure of the reconnection rate compared to the one described in Kowal et al. (2009), which in 2D is given by the simplified equation

$$V_{\rm rec} = \frac{1}{2|B_{x,\infty}|}\left[(\mathrm{sign}(B_x)E_z)\big|_{y_{\max}} - (\mathrm{sign}(B_x)E_z)\big|_{y_{\min}} - \partial_t \int_{y_{\min}}^{y_{\max}} \mathrm{d}y |B_x| \right], \quad (6)$$

where $|B_{x,\infty}|$ is the asymptotic absolute value of B_x and E_z is the Z component of the electromotive force. A more complete discussion of this new reconnection measure can be found in Kowal et al. (2009).

3. Results

3.1. Laminar reconnection

During the first stage of our simulations, before we start driving the turbulence, the system evolves to reach the stationary state of Sweet-Parker reconnection. After that the influence of turbulence on the evolution of our system can be studied in detail. As

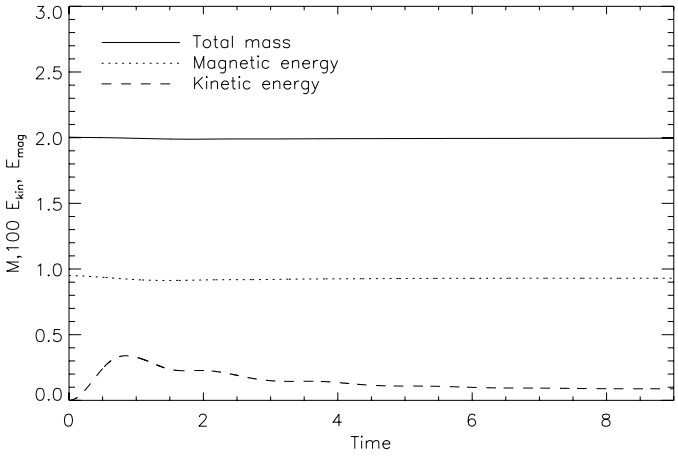

Fig. 2. Time variations of the total mass M (solid line), magnetic $E_{\rm mag}$ (dashed line) and kinetic $E_{\rm kin}$ (dotted line) energies in the Sweet-Parker reconnection stage with the uniform resistivity $\eta_{\rm u} = 5\times10^{-4}$. For clarity the kinetic energy $E_{\rm kin}$ has been amplified by a factor of 100.

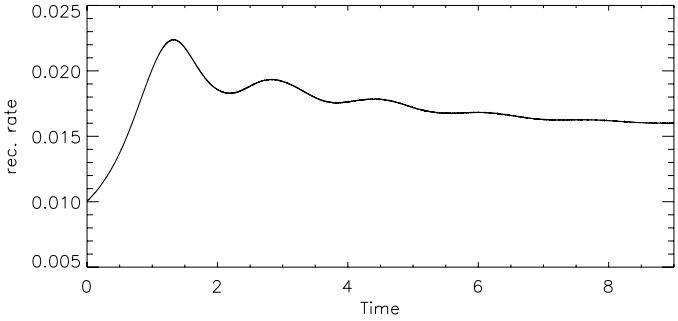

Fig. 3. Time variation evolution of the reconnection rate in the Sweet-Parker stage with the uniform resistivity $\eta_{\rm u} = 5 \times 10^{-4}$.

mentioned above we start our simulations with a configuration of the oppositely directed initial magnetic fields with a small magnetic perturbation. The perturbation initiates the Sweet-Parker reconnection which reaches a stationary state in a few Alfén time units which lasts until we start injecting turbulence.

We assume that we get the steady state of Sweet-Parker reconnection when the total mass, reconnection rate, kinetic and magnetic energies show very small time derivatives. Figure 2 shows the evolution of mass, kinetic and magnetic energy during the laminar reconnection stage. In the beginning all these quantities change slightly, but then reach almost constant values. The reconnection rate (Fig. 3) initially increases until $t \sim 1.3$, when it starts to oscillate, finally stabilizing after a few time units.

Figure 4 shows the topology of the velocity (left panel) and magnetic fields (middle panel), and the absolute value of the current density (right panel) just before we start injecting turbulence. The brighter shades correspond to high values of the displayed quantities. The velocity field and magnetic field are shown in the form of texture. The initial oppositely directed magnetic field lines are transported to the middle of the box. The Y-component of magnetic field emerges from the current sheet and is ejected near the midplane through the left and right boundaries. The reconnection process in the diffusion region and the ejection of B_y cause the strong outflow of gas which is clearly visible in the left panel of Fig. 4. The system reaches a steady state despite this loss of mass due to the inflow of gas through the top and bottom of the computational box.

The absolute value of the current density is shown in the right panel of Fig. 4. As expected the highest values of the current density appear in the midplane and determine the diffusion region. The state of the Sweet-Parker reconnection described above is stationary and sufficient to study the influence of turbulence on the reconnection process.

3.2. Reconnection in the presence of turbulence

In this section we present the influence of turbulence on the reconnection process. Turbulence was injected at a time $t = 9$ and at a given injection scale $l_{\rm inj} \propto k_{\rm f}^{-1}$ in the vicinity of the midplane. We gradually increased the strength of turbulence during one Alfvén time, thus at a time $t = 10$ the power reached its input value defined by $P_{\rm inj}$.

Figure 5 shows the reconnection rate obtained for a model with the uniform resistivity $\eta_{\rm u} = 5 \times 10^{-4}$, a turbulent power $P_{\rm inj} = 0.1$ and an injection wavenumber $k_{\rm f} = 12$. Adding turbulence to the system results in slight fluctuations of the reconnection rate until $t = 11.5$. Next, the reconnection rate increases significantly until it reaches the maximum at a time $t \sim 13$ and then drops. We can distinguish four of these maxima, which are roughly separated by two Alfvén times ($t \sim 13$, $t \sim 15$, $t \sim 17$, $t \sim 19$). In Fig. 5 we mark three time steps corresponding to the same time stages shown in Fig. 6, where we plot the current density, magnetic and gas velocity fields.

In Fig. 6 (top and middle row) we see that the structure of the magnetic and velocity fields are considerably different than in the case of the Sweet-Parker reconnection (see Fig. 4). At $t_1 = 12.15$ (Fig. 6, first column, top panel) we are injecting turbulence with the maximum power $P_{\rm inj} = 0.1$ in a large volume surrounding the the midplane. Thus the velocity field is strongly perturbed and mixed in this region. Although the topology of the velocity field is very complicated, we can distinguish the main direction of the velocity fluctuations, which is parallel to the mean magnetic field.

A smaller number of distinct features in the velocity field are pointed perpendicular to the mean magnetic field. Close to the midplane the magnetic field lines change their directions and are substantially reduced in strength. Thus, velocity fluctuations can bend magnetic field lines in this region. Another noticeable difference in comparison to the Sweet-Parker configuration is a significant change of the current density distribution. Adding turbulence to the system creates a very complex configuration of the magnetic field, so that we observe multiple reconnection events happening at the same time (Fig. 6, $t_1 = 12.15$, bottom panel).

The magnetic field configuration looks quite different at the next time step $t_2 = 13.85$ (Fig. 6, second column, middle panel). In the vicinity of the midplane we observe the formation of a magnetic island. The velocity field (Fig. 6, second column, top panel) is also more mixed in this region. However, the outflow velocity of the gas velocity is quite low, which is confirmed by the small reconnection rate (Fig. 5).

As the simulation proceeds a large loop of magnetic field lines moves to the left boundary (Fig. 6, $t_3 = 15.15$, last column). This causes a powerful outflow of gas, which results in a violent and rapid growth of the reconnection rate (Fig. 5). We see that the maxima of the velocity field associated with this loop are where the value of magnetic field is low. The area of the magnetic island $t_2 = 13.85$ and $t_3 = 15.15$ is also well defined by the current density distribution (Fig. 6, bottom panel, middle and right column).

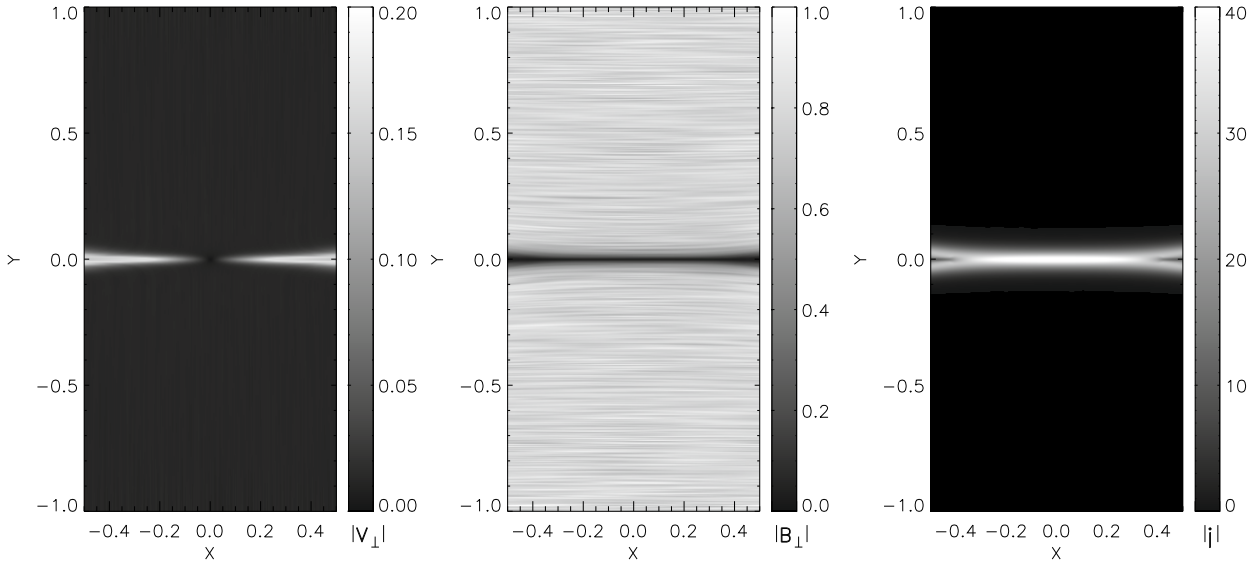

Fig. 4. Absolute value of the current density distribution (*right panel*), the magnetic (*middle panel*) and velocity field (*left panel*) topology during the Sweet-Parker stage for a time $t = 9$ in a model with the uniform resistivity $\eta_u = 5 \times 10^{-4}$. Brighter shades correspond to the higher values of the displayed quantities. All panels show the moment just before we start injecting turbulence.

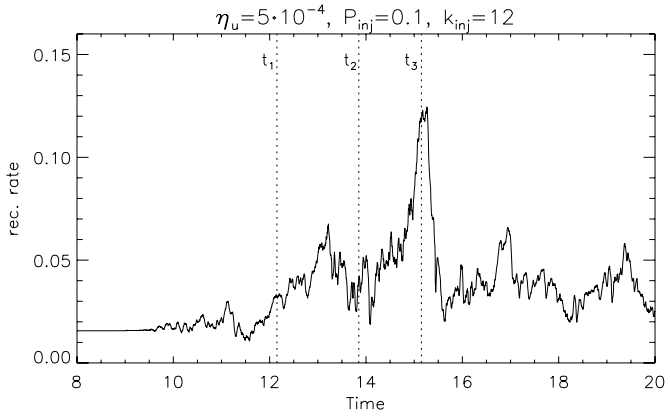

Fig. 5. The evolution of the reconnection speed for a model with $P_{inj} = 0.1$, a mean wavenumber of the injected turbulence $k_f = 12$ and uniform resistivity $\eta_u = 5 \times 10^{-4}$. Marked time steps correspond to those presented in Fig. 6.

Figure 7 shows the evolution of the reconnection speed for $P_{inj} = 0.5$, five times larger than in the previous case. As before the reconnection rate does not reach a stationary state. We observe a few maxima, but they do not appear periodically as in the previous case (Fig. 5). In fact, we have two main well defined maxima at times $t \sim 14.6$ and $t \sim 19.5$. The peak in the reconnection speed is again caused by a fast outflow of gas visible at a time $t_1 = 13.90$ in Fig. 8 (first column, top panel). If we look at the magnetic field topology at the same time (Fig. 8 first column, middle panel), we see a magnetic island which appears in the region of the fast outflow.

At the next time step ($t_2 = 15.70$) the topology of magnetic and velocity fields are still very mixed and complex (Fig. 8, second column, top and middle panel), but the magnetic field does not exhibit the very strong bending seen in the previous step. As the simulation proceeds the reconnection rate slowly decreases, reaching even slightly negative values[1] (Fig. 7, from $t \sim 16$ to $t \sim 18.5$).

[1] This should not be taken too literally. Our measure of the reconnection speed is misleading when the midplane magnetic field topology becomes progressively more tangled.

At the time step $t_3 = 18.15$ (Fig. 8, last column) we show how our model looks when the measured reconnection rate is negative. We can see a strong accumulation of the magnetic field around the midplane which extends over almost the whole computational domain. The region of velocity fluctuations is broadened in comparison to the previous time steps, even though the volume within which we drive turbulence is unchanged. This quite unstable situation sets off the extreme growth of the reconnection rate (from $t \sim 18.5$ to $t \sim 19.5$) shown in Fig. 7. The current density distribution is plotted in the bottom row in Fig. 8. At every time step many small reconnection events occur, as indicated by the local growth of the current density.

To verify the influence of magnetic islands on the overall recconection rate we calculated the mean reconnection rate in the two defined periods of time. First, when the magnetic island is presented in the computational domain (from $t = 13.5$ to $t = 15.5$ for the model with $P_{inj} = 0.1$ and from $t = 13.5$ to $t = 15.0$ for model with $P_{inj} = 0.5$) and second, when magnetic islands do not appear (from $t = 17.0$ to $t = 19.0$ for the model with $P_{inj} = 0.1$ and from $t = 15.0$ to $t = 16.0$ for the model with $P_{inj} = 0.5$). For the magnetic islands created in the domain and subsequently ejected through the boundaries, the mean reconnection rate is equal to $V_r = 0.059 \pm 0.027$ and $V_r = 0.105 \pm 0.042$ for models with $P_{inj} = 0.1$ and $P_{inj} = 0.5$, respectively. On the other hand, when we do not observe any magnetic island the corresponding reconnection rates are $V_r = 0.034 \pm 0.006$ and $V_r = 0.052 \pm 0.013$ for models with $P_{inj} = 0.1$ and $P_{inj} = 0.5$, respectively. Comparing these values with the overall reconnecton rate ($V_r = 0.039 \pm 0.019$ for $P_{inj} = 0.1$ and $V_r = 0.064 \pm 0.062$ for $P_{inj} = 0.5$) we notice that the magnetic islands do not lead to a significant growth of the reconnection pace but are the sources of the very large fluctuations.

3.2.1. Dependence on the strength of turbulence

To check how the reconnection rate V_t^{TB} depends on the strength of turbulence we made several simulations with different values of the turbulent power P_{inj} (see model PD in Table 1). The rest of the input parameters had the same value in all these models.

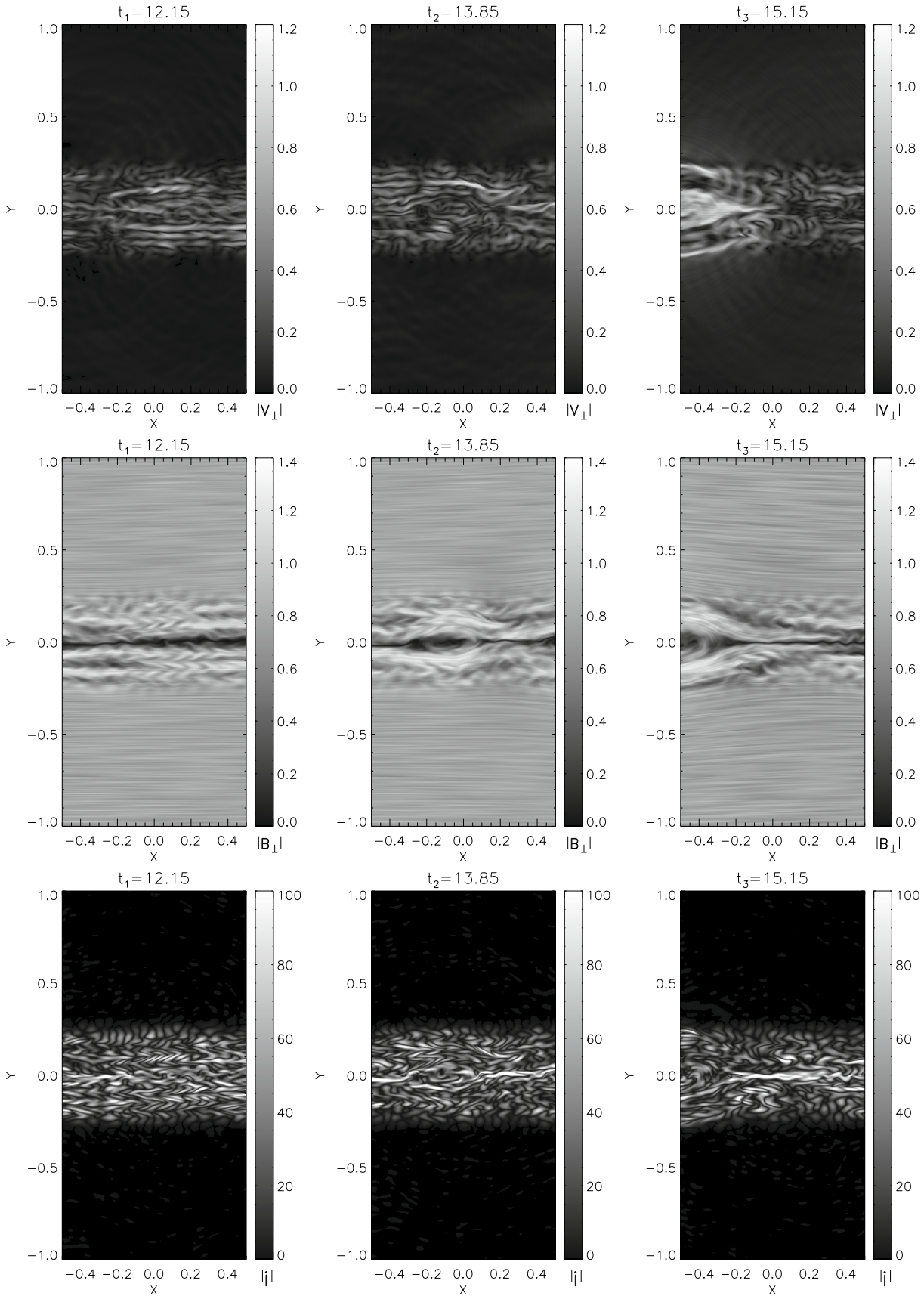

Fig. 6. Topology of the velocity (*top panels*) and magnetic field (*middle panels*) in the presence of turbulence shown at three times $t_1 = 12.15$, $t_2 = 13.85$, $t_3 = 15.15$. In the *lower panels* we plot the absolute value of the current density at these times. The variation of the reconnection speed $V_r^{\rm TB}$ for this model is presented in Fig. 5. Turbulence is injected with a power $P_{\rm inj} = 0.1$ and at a scale $k = 12$. The uniform resistivity $\eta_{\rm u}$ is equal to 5×10^{-4}. The brighter shades correspond to the higher values of the displayed quantities.

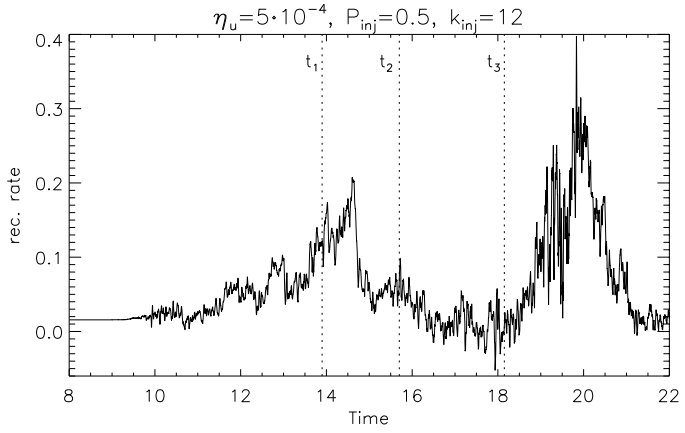

Fig. 7. The evolution of the reconnection speed for the model with $P_{\rm inj} = 0.5$, injection scale $k_{\rm f} = 12$ and uniform resistivity $\eta_{\rm u} = 5 \times 10^{-4}$. Marked times correspond to those shown in Fig. 8.

In Fig. 9 we present the dependence of the averaged reconnection speed on the power of the injected turbulence. Diamonds and squares correspond to the reconnection rate with and without the turbulence respectively. Both were averaged over the fixed period of time: from $t = 7$ to $t = 9$ – laminar reconnection (Sweet-Parker stage) and from $t = 10$ to $t = 20$ – turbulent reconnection. The variance of the reconnection rate was calculated with the standard deviation method. For the Sweet-Parker reconnection the variance is negligible and is not shown here. On the other hand, in the presence of turbulence the reconnection rate undergoes continuous strong variations, and the variance is only slightly smaller than the mean reconnection rate. We find that the reconnection rate increases with the power of turbulence and scales as $\sim P_{\rm inj}^{1/3}$.

3.2.2. Dependence on the injection scale

Similarly we determined the dependence of the reconnection rate $V_r^{\rm TB}$ on the wavenumber at which we inject turbulence $k_{\rm f}$. We computed several models with varying $k_{\rm f}$ while keeping all other parameters the same (see model PD in Table 1).

Figure 10 shows the resulting dependence. We can clearly see the strong relation between the injection scale $k_{\rm f}$ and the reconnection speed, i.e. the reconnection rate and errors increase with a decreasing injection wavenumber $k_{\rm f}$. Fitting to the simulation results gives $V_r^{\rm TB} \sim l_{\rm inj}^{2/3}$.

3.2.3. Dependence on the resistivity

The most important goal in our study was to check the dependence of the reconnection rate on the uniform resistivity. We run several simulations with different values of the uniform resistivity $\eta_{\rm u}$ and the power of turbulence $P_{\rm inj}$ (see model RD in Table 1).

In Fig. 11 we plot the obtained dependence of reconnection rate on uniform resistivity. For the Sweet-Parker configuration the averaged reconnection rate $V_r^{\rm SP}$ is represented by squares. The dispersion of the calculated points is almost negligible and not shown. As we can see the reconnection speed $V_r^{\rm SP}$ increases with uniform resistivity. From the fitting we obtain that the reconnection rate $V_r^{\rm SP}$ scales with the uniform resistivity as $\sim \eta_{\rm u}^{1/2}$. This agrees with the theoretical prediction (Sweet 1958; Parker 1957) and confirms that our 2D model works well in the laminar reconnection stage.

Adding turbulence to the system leads to a weaker dependence between the reconnection rate and the uniform resistivity. Moreover, the power of turbulence also influences this relationship, as is clearly visible in Fig. 11 (triangles – $P_{\rm inj} = 0.01$, squares – $P_{\rm inj} = 0.1$). We fit lines to calculated points and find that the dependence between reconnection rate and uniform resistivity is stronger for lower values of $P_{\rm inj}$. Namely, for $P_{\rm inj} = 0.1$ and $P_{\rm inj} = 0.01$ we see that the reconnection rate scales as $\sim \eta_{\rm u}^{1/5}$ and $\sim \eta_{\rm u}^{1/3}$, respectively.

For low values of the uniform resistivity ($\eta_{\rm u} \leq 1 \times 10^{-3}$–$P_{\rm inj} = 0.1$ and $\eta_{\rm u} \leq 7 \times 10^{-4}$–$P_{\rm inj} = 0.01$) we see that the obtained reconnection speeds $V_r^{\rm TB}$ are almost the same. These similar values of the reconnection rate may be caused by prevailing numerical diffusion. Even if we take into account higher values of $\eta_{\rm u}$, it does not modify the overall value of the total resistivity. However, in this case the numerical diffusion will also influence the reconnection rate in the Sweet-Parker configuration, which does not happen in our simulations (see Fig. 11).

Results described above indicate that in 2D turbulent reconnection depends on the uniform resistivity. However, the obtained dependencies are not certain because of the large dispersion of results for low values of the uniform resistivity $\eta_{\rm u}$.

We also tested the dependence of the reconnection rate on the anomalous resistivity. We run several models with the same value of the uniform resistivity $\eta_{\rm u} = 5 \times 10^{-4}$ and the critical current density $j_{\rm crit} = 50$, but for different values of the anomalous resistivity $\eta_{\rm a}$ (see model AD in Table 1). In Fig. 12 we plot the reconnection rate calculated for the Sweet-Parker configuration (squares) and in the presence of turbulence (diamonds). The dash-dotted line determines the mean value of the reconnection rate ($V_{r\,(\eta_{\rm a}\neq 0)}^{\rm TB} = 0.051$) obtained for models with the anomalous resistivity. As we see, the presence of anomalous resistivity causes an increase in the reconnection speed compared to a model with $\eta_{\rm a} = 0$ – dotted line ($V_r^{\rm TB} = 0.039$). However, for different values of the anomalous resistivity the reconnection speed is almost the same. More precisely, we observe a nearly negligible increase in the reconnection rate and a clear increase in the variance at higher values of the anomalous resistivity $\eta_{\rm a}$.

3.3. Dependence on the viscosity

In a next step we tested the influence of viscosity on the reconnection rate for fixed values of the injection scale, turbulence strength and uniform resistivity (see model VD in Table 1). The results are shown in Fig. 13 where we plot averaged reconnection rates for the laminar (squares) and turbulent (diamonds) cases. In the Sweet-Parker configuration the reconnection rate $V_r^{\rm SP}$ is almost the same for viscosity $\nu \leq 1 \times 10^{-3}$ and starts to decrease for $\nu \geq 2 \times 10^{-3}$. In the presence of turbulence the fit to the calculated points shows that the reconnection rate $V_r^{\rm TB}$ scales with the viscosity as $\sim \nu^{-1/3}$. Furthermore, when the viscosity is higher than 1×10^{-3}, the rates of reconnection for models with and without turbulence are similar.

3.4. The case of a uniform initial configuration

To check the influence of our boundary conditions and method of driving turbulence on the reconnection process we compare two models with different initial magnetic field configurations: antiparallel and uniform. The antiparallel initial configuration of the magnetic field is the same as for the Sweet-Parker reconnection, the uniform one is horizontal with $B_x = 1$. The rest of the parameters characterizing both models are $\eta_{\rm u} = 5 \times 10^{-4}$,

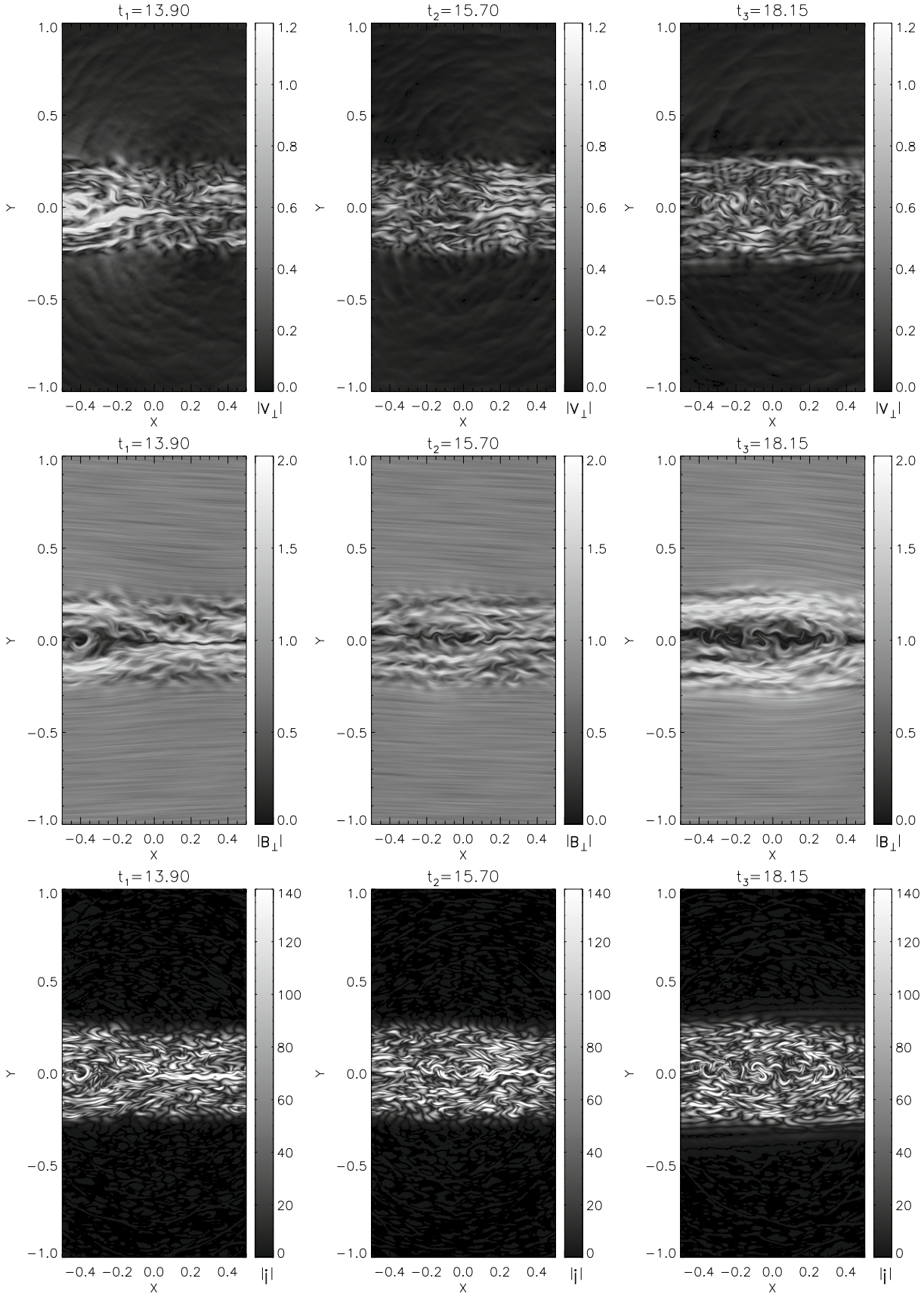

Fig. 8. Topology of the velocity (*top panels*) and magnetic field (*middle panels*) in the presence of turbulence shown at three times $t_1 = 13.90$, $t_2 = 15.70$, $t_3 = 18.15$. In the *lower panels* we plot the absolute value of the current density for the same times. The evolution of the reconnection speed $V_r^{\rm TB}$ for this model is shown in Fig. 7. Turbulence is injected with $P_{\rm inj} = 0.5$ at the wavenumber $k = 12$. The uniform resistivity $\eta_{\rm u}$ is equal to 5×10^{-4}. Brighter shades correspond to higher values of the displayed quantities.

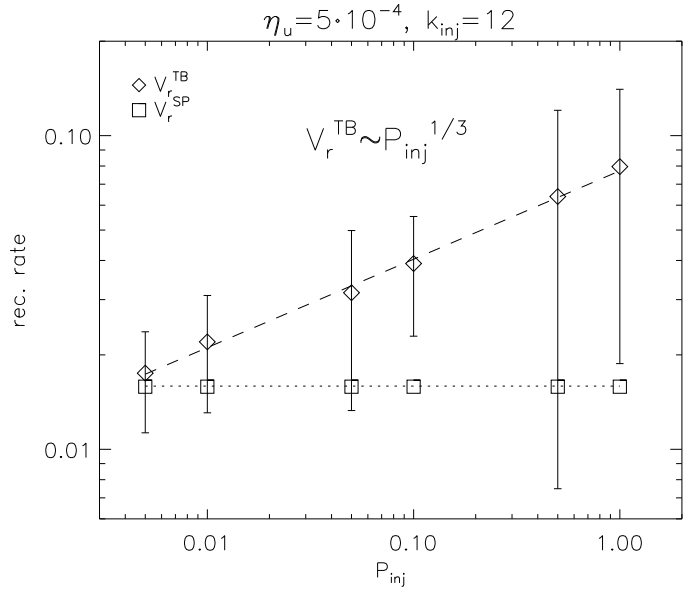

Fig. 9. Dependence of the reconnection rate on the power of the injected turbulence $P_{\rm inj}$ for models with and without turbulence, $V_r^{\rm TB}$ and $V_r^{\rm SP}$, respectively. In all models we use the same values of the uniform resistivity $\eta_{\rm u} = 5 \times 10^{-5}$ and the injection scale $k_{\rm inj} = 12$. The error bars indicate the variance of the reconnection rate. For the Sweet-Parker reconnection (squares) the errors are neglected and not shown.

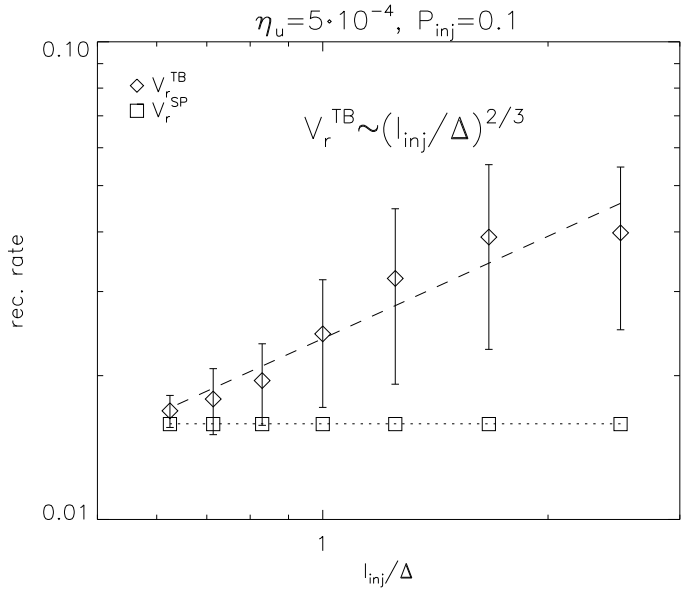

Fig. 10. Dependence of the reconnection rate on the injection scale $l_{\rm inj}$ for models with and without turbulence, $V_r^{\rm TB}$ and $V_r^{\rm SP}$, respectively. In all models we use the same values of the uniform resistivity $\eta_{\rm u} = 5 \times 10^{-5}$ and the power of the injected turbulence $P = 0.1$. For the Sweet-Parker reconnection (squares) the variance is negligible and not shown.

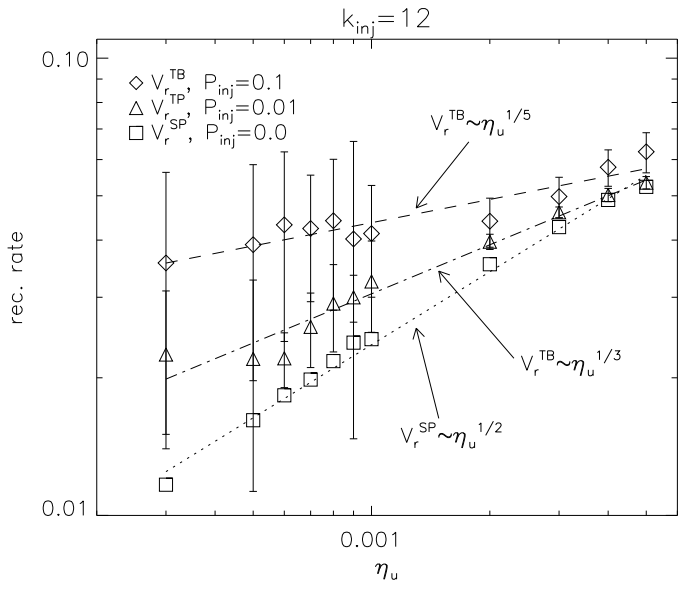

Fig. 11. Dependence of the reconnection rate on the uniform resistivity $\eta_{\rm u}$ for models with and without turbulence, $V_r^{\rm TB}$ (diamonds and triangles) and $V_r^{\rm SP}$ (squares), respectively. Turbulence is injected at the scale $k = 12$ with $P_{\rm inj} = 0.1$ and $P_{\rm inj} = 0.01$. For the Sweet-Parker reconnection (squares) the variance is negligible and not shown.

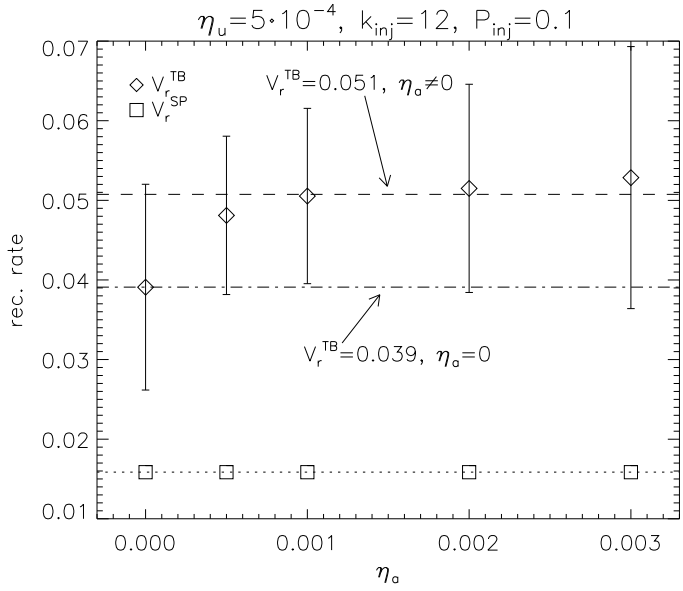

Fig. 12. Dependence of the reconnection rate on the anomalous resistivity $\eta_{\rm a}$ for models with and without turbulence, $V_r^{\rm TB}$ (diamonds) and $V_r^{\rm SP}$ (squares), respectively. Turbulence is injected at the wavenumber $k_{\rm f} = 12$ with $P_{\rm inj} = 0.1$. The uniform resistivity $\eta_{\rm u}$ is equal to 5×10^{-4}. The dotted line represents the mean reconnection rate obtained for the Sweet-Parker stage, dash-dotted marks the value of the reconnection rate without anomalous resistivity and the dashed line corresponds to the mean reconnection rate calculated for four models with different values of the anomalous resistivity.

$k_{\rm f} = 12$, $P = 0.1$ and inflow/outflow boundary conditions. In both models we injected turbulence in the same way from $t = 9$ to $t = 10$.

In Fig. 14 we show the comparison of reconnection rates obtained for the uniform and antiparallel initial magnetic field configuration. In the first case the reconnection rate is almost equal zero. We can see some small fluctuations, but we cannot observe any significant growth of the reconnection rate. In the second case the value of reconnection rate is higher and changes violently. For a more precise description of this case see Sect. 3.2.

The almost negligible value of the reconnection rate for the model with a uniform initial magnetic field indicates that as expected magnetic reconnection does not occur. This also supports the conclusion that our calculation of the reconnection rate is not

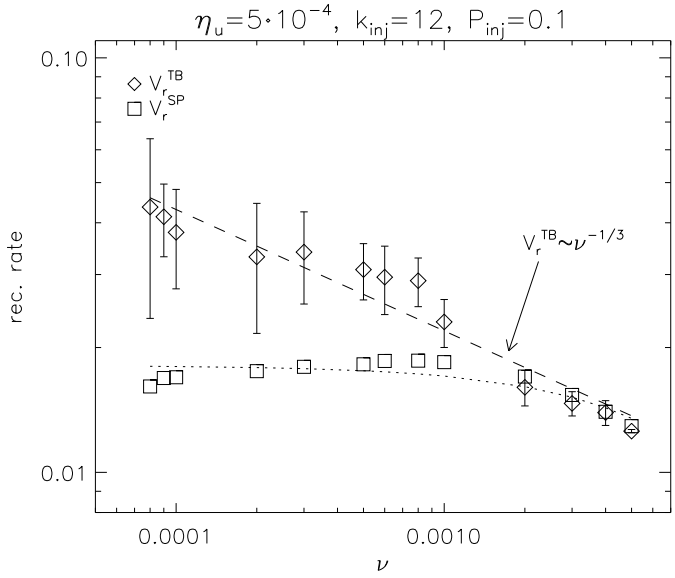

Fig. 13. Dependence of the reconnection rate on the viscosity ν for models with and without turbulence, $V_r^{\rm TB}$ and $V_r^{\rm SP}$, respectively. In all models we use the same values of the uniform resistivity $\eta_{\rm u} = 5 \times 10^{-5}$, turbulence strength $P = 0.1$ and the injection wavenumber $k_{\rm inj} = 12$. For the Sweet-Parker reconnection (squares) the variance is negligible and not shown.

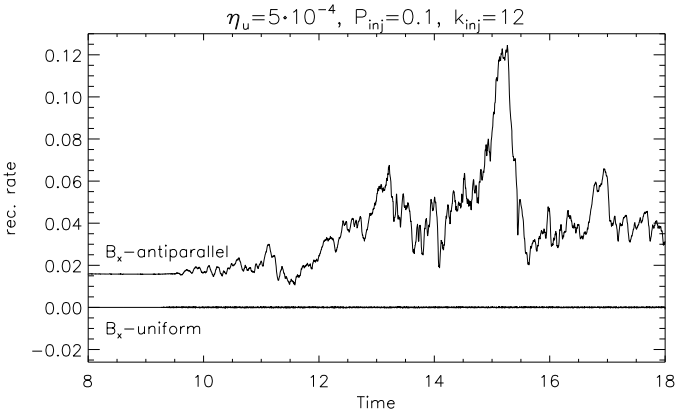

Fig. 14. Comparison of the reconnection rates obtained for models with uniform and antiparallel initial magnetic field configurations. All parameters for the models are the same: the power of turbulence $P_{\rm inj} = 0.1$, the injection wavenumber $k_{\rm f} = 12$, and the uniform resistivity coefficient $\eta_{\rm u} = 5 \times 10^{-4}$. The topology of the velocity and magnetic velocity fields as well as the distribution of the current density for both models are shown in Fig. 6 (antiparallel initial magnetic field) and Fig. 15 (uniform initial magnetic field).

an artifact of our boundary conditions or our method for implementing turbulence.

Figure 15 shows the topology of the magnetic and velocity field as well as the distribution of current density for the model with an initial uniform configuration of the magnetic field. As before turbulence was injected in a volume surrounding the midplane, which causes perturbations of the velocity field in this region (see the left panel in Fig. 15). Most of the fluctuations propagate along the mean magnetic field, running more or less parallel to the midplane (see the middle panel in Fig. 15). The well defined bend of the magnetic lines presented in the case of turbulent reconnection is not visible here. This is because we do not have a diffusion region, where the magnetic lines change their direction and strength and can be bent by fluctuations. On the other hand, turbulence causes small perturbations of magnetic field, which leads to an enhancement of the absolute value of the current density (see the middle panel in Fig. 15).

3.5. Long term variance of the reconnection rate

The time evolution of the reconnection rate for the same model as in Fig. 5 but calculated over a longer period of time ($t_{\rm end} = 50$) is shown in Fig. 16. We see that even after 50 Alfénic times the reconnection rate does not reach a steady state. Strong and continuous fluctuations are seen over the whole simulation time. All these quasiperiodic changes of the reconnection rate are apparently driven by something like the tearing mode instability, namely, big loops of magnetic field are continuously created (see Fig. 18) and ejected through boundaries.

In Fig. 17 we show the evolution of mass, magnetic and kinetic energy during the Sweet-Parker reconnection (from $t = 0$ to $t = 9$) and turbulent (from $t = 9$ to $t = 50$) reconnection. We see that adding turbulence to the system or using open boundary conditions does not introduce instabilities in the total mass or kinetic and magnetic energies.

What is more, increasing $t_{\rm end}$ from 20 to 50 only slightly influences the average reconnection rate and its variance. For models with $t_{\rm end} = 20$ and $t_{\rm end} = 50$ we get $V_r^{\rm TB} = 0.039 \pm 0.019$ and $V_r^{\rm TB} = 0.041 \pm 0.017$, respectively. This indicates that extending the simulation time does not lead to a stable state of reconnection and does not change our results.

4. Discussion

4.1. The goals of this study

The present paper provides a follow-up study to Kowal et al. (2009). In that paper fast magnetic reconnection of a 3D weakly stochastic magnetic field, predicted in the LV99 theoretical study, was confirmed. Can turbulent reconnection be fast in 2D as well? The question may sound rather academic, as the nature we deal with is definitely three dimensional. However, there are at least two reasons why answering this question is important. First of all, the claim in LV99 is that 3D effects are essential for fast reconnection. Thus it is important to test this claim and to explore whether fast reconnection in the presence of turbulence can be carried over to 2D. Then, in a number of earlier studies it was conjectured that magnetic reconnection could become fast in the presence of turbulence for purely 2D reconnection configurations.

In all respects apart from dimensionality the present numerical set-up is identical to that in Kowal et al. (2009). In particular, the excitation of turbulence in both cases takes place at subAlfvénic velocities, thereby preventing field reversals arising from turbulence. For measurements of the reconnection rate we adopt the procedure presented in Kowal et al. (2009). This enables us to make easy comparisons between the 3D and 2D reconnection results.

4.2. 2D versus 3D reconnection

Until very recently 2D geometry has been favored for magnetic reconnection studies. Its advantage stems from the fact that it allows one to achieve much higher Lundquist numbers compared to its 3D counterpart. The most important question is whether the nature of reconnection is the same in 3D and in 2D. An affirmative answer is likely if the reconnection of laminar magnetic

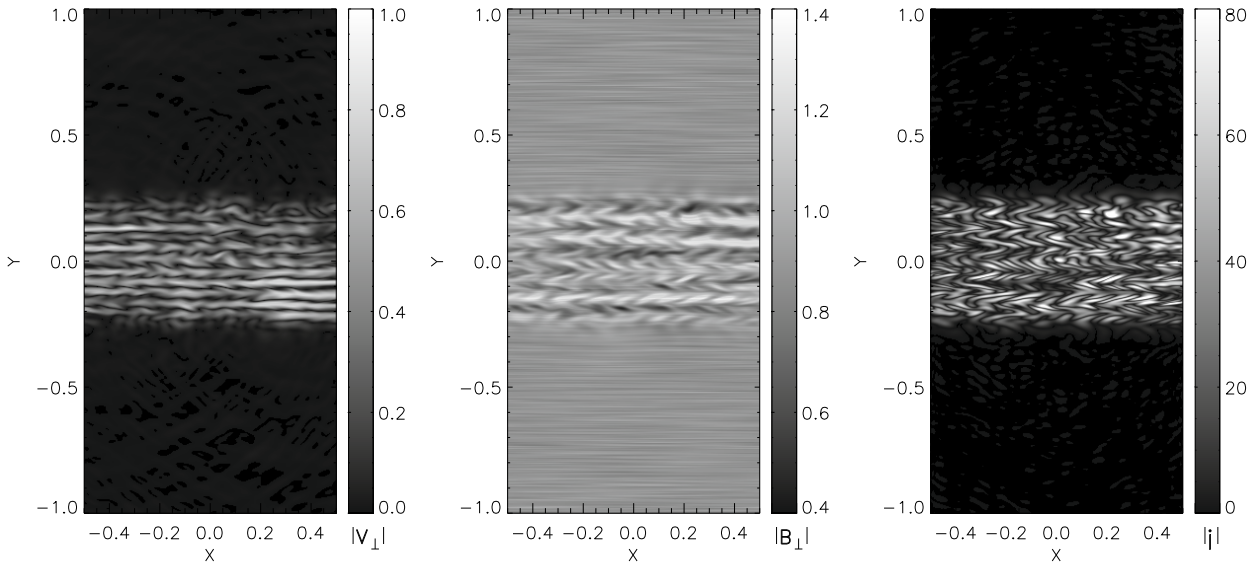

Fig. 15. Topology of the velocity (*left panel*) and magnetic field (*middle panel*), and the absolute value of the current density distribution (*right panel*) for the initially uniform magnetic field at the time $t = 14$. Brighter shades correspond to higher values of the displayed quantities. Turbulence is injected with the power $P_{\rm inj} = 0.1$ at a wavenumber $k_{\rm f} = 12$. The uniform resistivity $\eta_{\rm u}$ is equal to 5×10^{-4}. For comparison, the model with the same set of parameters but with an initially antiparallel configuration of magnetic field is presented in Fig. 6.

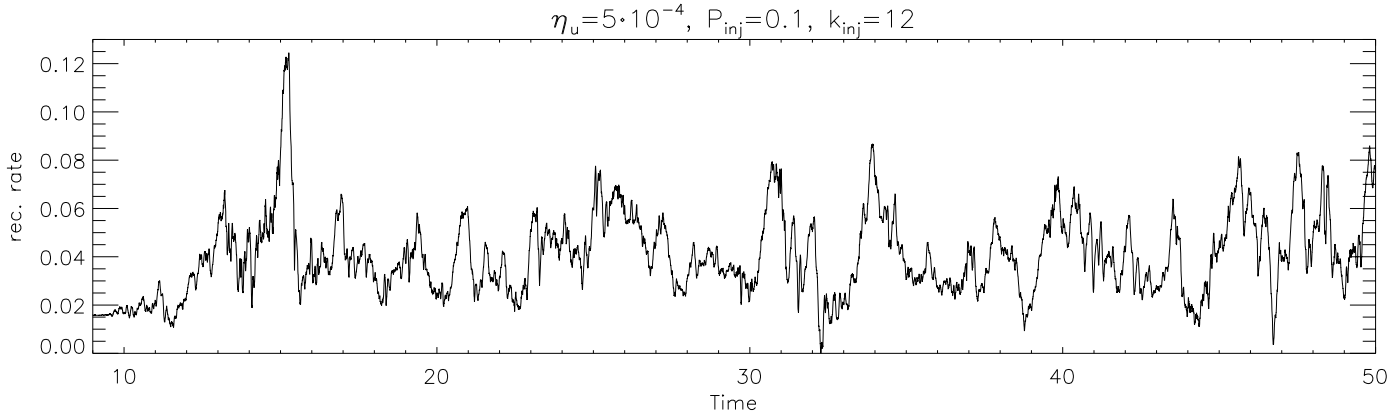

Fig. 16. Time evolution of the reconnection speed for the model with t $P_{\rm inj} = 0.1$, an injection wavenumber $k_{\rm f} = 12$ and a uniform resistivity $\eta_{\rm u} = 5 \times 10^{-4}$.

field is involved. Our results on the Sweet-Parker reconnection above are very similar[2] to the results of the Sweet-Parker reconnection in Kowal et al. (2009). At the same time our comparison of the results in the present paper with those in Kowal et al. (2009) shows that the reconnection in the presence of turbulence is very different.

The aforementioned difference is not surprising if one takes into account that the nature of the 2D and 3D MHD turbulence is rather different. In particular, magnetic field wandering, which is an essential part of the LV99 reconnection model, has a radically different nature in 3D and 2D. What we have in 2D is a coherent displacement of magnetic field lines by Alfvénic perturbations, while in 3D magnetic field lines can slip past one another, enjoying the freedom provided by the additional dimension. As a result, in LV99 different bundles of wandering magnetic field lines can enter the reconnection zone independently, and reconnect simultaneously. It was shown in LV99 that it is this simultaneous reconnection of independent magnetic flux bundles that makes reconnection insensitive to resistivity. This effect is absent in 2D, where the entry of fresh flux into the reconnection zone is constrained by the rate of removal of reconnected flux.

The second effect that enables fast reconnection in the LV99 model is an increase of the thickness of the outflow region. There we see some similarity between 2D and 3D reconnection. Indeed, while the outflow in the Sweet-Parker reconnection is constrained by the thin slot determined by Ohmic diffusivity, it is due to an increase of the thickness of the outflow through turbulence that 2D turbulent reconnection is faster than the Sweet-Parker rate. The outflow region for both 2D and 3D depends on the intensity of driving and the scale of turbulence injection. However, the functional dependencies are different, and this difference stems from the difference in the reconnection physics.

As we mentioned earlier, magnetic field wandering plays a decisive role in 3D reconnection. In 2D reconnection it is not fast, since we observe the creation of magnetic islands as a result of turbulence. This process is rather limited unless the turbulent injection velocity approaches $V_{\rm A}$. We believe that this

[2] The obtained dependence of reconnection pace on the uniform resistivity coincide in 2D and 3D and is consistent with theory, i.e. $V_r^{\rm SP} \sim \eta_{\rm u}^{1/2}$.

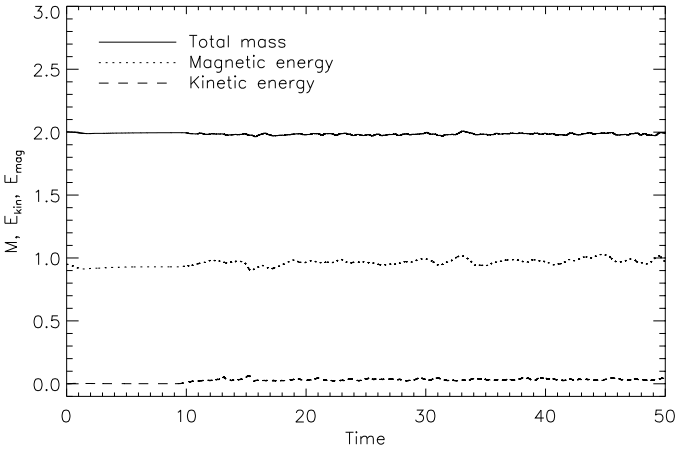

Fig. 17. Time evolution of the total mass M (solid line), magnetic $E_{\rm mag}$ (dashed line) and kinetic $E_{\rm kin}$ (dotted line) energies during the Sweet-Parker reconnection (from $t = 0$ to $t = 9$) and turbulent (from $t = 9$ to $t = 50$ reconnection with a uniform resistivity $\eta_{\rm u} = 5\times10^{-4}$. The kinetic energy $E_{\rm kin}$ is not amplified in this plot.

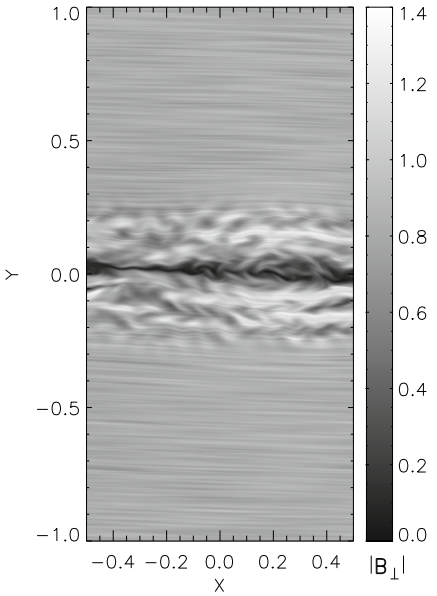

Fig. 18. Topology of magnetic field in the presence of turbulence at a time $t = 49$. The uniform resistivity $\eta_{\rm u}$ is equal to 5×10^{-4}. Turbulence is injected with the power $P_{\rm inj} = 0.1$ at a scale $k = 12$. Brighter shades correspond to higher values of the displayed quantities.

explains why the dependence of the reconnection rate on the Ohmic resistivity becomes steeper as the turbulence weakens (see Fig. 11). Indeed, for a weaker turbulence the alternate compression and expansion of the current sheet, which leads to magnetic island formation, is weaker and the reconnection is similar to the Sweet-Parker model. Similarly, the combination of anomalous resistivity and magnetic island formation[3] reaches a saturated level of efficiency for modest values of the anomalous resistivity and appears to become insensitive to further increases (see Fig. 12).

It is important to note that magnetic field structures, i.e. the magnetic islands, which we observe in 2D simulations do not appear in 3D simulation (Kowal et al. 2009). What is more, Kowal et al. (2009) obtained a stable value of the reconnection speed in the presence of turbulence in a short period, about one Alvén time. In our work we are unable to reach this state because the reconnection rate continuously and violently fluctuates. Consequently the average speed of turbulent magnetic reconnection in 2D is burdened with much higher statistical errors than in 3D.

In our work we determine the dependence of the reconnection rate on four quantities: the power of turbulence $P_{\rm inj}$, the injection wavenumber $k_{\rm f}$, the uniform $\eta_{\rm u}$ and the anomalous $\eta_{\rm a}$ resistivities. The same analysis was done by Kowal et al. (2009) in three dimensions. For the power of turbulence and injection scale they found the following scalings: $V_r^{\rm TB} \sim P_{\rm inj}^{1/2}$ and $V_r^{\rm TB} \sim l_{\rm inj}^{3/4}$. Compared to our findings the dependencies obtained in 3D are stronger. Namely, in the 2D case the reconnection rate grows with the power of turbulence as $V_r^{\rm TB} \sim P_{\rm inj}^{1/3}$ and with the injection scale as $V_r^{\rm TB} \sim l_{\rm inj}^{2/3}$.

4.3. Earlier studies of 2D turbulent reconnection and their relation to work

As we mentioned in the introduction, the concept of turbulent enhancement of reconnection is not unprecedented. In Kowal et al. (2009) we presented a list of papers where turbulent effects were cited as the source of fast astrophysical reconnection. Compared to the present paper, all these papers lacked a precise means of measuring the reconnection speed, and therefore the numerical simulations were providing mostly qualitative results. Moreover, they adopted periodic boundary conditions, which made it difficult to study turbulent reconnection for more than a single Alfvén time.

Among these papers, the pioneering works were the numerical studies in Matthaeus & Lamkin (1985, 1986). There the analysis of 2D simulations of turbulence revealed the formation of magnetic islands and X-points reminiscent of the Petscheck process.

In our 2D model of turbulent reconnection we also observe the continuous formation of magnetic islands which are ejected from the reconnection zone due to open boundary conditions. For instance, we observe that when a big loop of the magnetic field is removed from the box through boundaries, the reconnection rate increases sharply. After that the reconnection rate drops until a new magnetic island can be created.

The formation of islands is also a consequence of the tearing instability. In this vein, Loureiro et al. (2005) examined the nonlinear growth of tearing modes and obtained a fast growth of magnetic islands. However, in their simulations they used periodic boundary conditions, which keep such islands in the reconnection zone.

The most directly relevant work is Fan et al. (2004, 2005). They found that the turbulent magnetic reconnection in the solar atmosphere could be described by a two phase process: first-slow and second-fast. The rapid stage of reconnection is caused by the coalescence instability described in Biskamp & Welter (1980); Wu & Chang (2001), which may also enhance the reconnection rate in our simulations.

Here, and in contrast to the 3D model of LV99, we find that in 2D the influence of the uniform resistivity on the reconnection rate is stronger for higher values of $\eta_{\rm u}$ and lower values of $P_{\rm inj}$. Similar results have also been obtained by Loureiro et al. (2009). They claimed that the reconnection process is fast in 2D only in some particular circumstances, i.e. for higher values of the

[3] While the 3D reconnection of a weakly stochastic magnetic field depends on the Alfvénic, i.e. the incompressible, component of magnetic turbulence, the creation of magnetic islands depends on the compressible component of the turbulence (see Cho & Lazarian 2003, for the decomposition of MHD turbulent motions).

Lundquist number and moderate levels of turbulence. We disagree with the claim of fast turbulent reconnection in 2D. In fact, in most of the models analyzed by Loureiro et al. (2009) the reconnection process depends on the uniform resistivity. Again an important limitation of the aforementioned study is their limited averaging, arising from their choice of boundary conditions.

4.4. Implications

Two-dimensional magnetic reconnection is the result of a rather artificial configuration. The value of our present study is that it clarifies the role of the effects of dimensionality for the actual 3D reconnection of astrophysical magnetic fields in the presence of weak turbulence. The latter has many essential implications starting from the First Order Fermi acceleration of energetic particles (de Gouveia dal Pino & Lazarian 2005; Lazarian & Opher 2009) to Solar Flares (see Lazarian et al. 2009) and the removal of the magnetic field during star formation (Santos-Lima et al. 2010) These implications are discussed in more detail in Kowal et al. (2009).

5. Conclusions

In this paper we have examined the results of 2D simulations of the reconnection process in the presence of subAlfvenic turbulence. Our findings may be summarized as follows:

- Unlike the Sweet-Parker reconnection, the reconnection of a weakly stochastic magnetic field is fundamentally different in 2D and 3D, in agreement the LV99 study. Reconnection in 2D depends on resistivity and is not fast.
- The enhancement of magnetic reconnection in 2D arises from an increase in the thickness of the plasma outflow layer due to the creation of magnetic islands, which are ejected from the reconnection layer.
- The power of turbulence $P_{\rm inj}$ and the injection scale $k_{\rm f}$ have an influence on the reconnection rate. In our study this is $V_r^{\rm TB} \sim P_{\rm inj}^{1/3} \sim l_{\rm inj}^{2/3}$.

Acknowledgements. This work of K.K. and K.O. was supported by the Polish Ministry of Science and Higher Education through grants: 92/N-ASTROSIM/2008/0 and 3033/B/H03/2008/35. G.K.'s work was supported by the Polish Ministry of Science and Higher Education through 3033/B/H03/2008/35 and by the National Science Foundation through AST 0808118. The work of A.L. was supported by AST 0808118 and ATM 0648699. The work by E.V. was supported National Science and Engineering Research Council of Canada. The computations presented here have been performed on the GALERA supercomputer in TASK Academic Computer Centre in Gdańsk.

References

Alvelius, K. 1999, Phys. Fluids, 11, 1880
Armstrong, J. W., Rickett, B. J., & Spangler, S. R. 1995, ApJ, 443, 209
Biskamp, D. 1996, Ap&SS, 242, 165
Biskamp, D., & Welter, H. 1986, Phys. Rev. Lett., 44, 1069
Blackman, E. G., & Field, G. B. 2000, ApJ, 534, 984
Blackman, E. G., & Field, G. B. 2008, MNRAS, 386, 1481
Cattaneo, F., & Vainshtein, S. I. 1991, ApJ, 376, L21
Cho, J., & Lazarian, A. 2003, MNRAS, 345, 325
Del Zanna, L., Bucciantini, N., & Londrillo, P. 2003, A&A, 400, 397
Drake, J. F., Swisdak, M., Che, H., & Shay, M. A. 2006, Nature, 443, 553
Elmegreen, B. G., & Scalo, J. 2004, ARA&A, 42, 211
Fan, Q.-L., Feng, X.-S., & Xiang, C.-Q. 2004, Phys. Plasmas, 12, 052901
Fan, Q.-L., Feng, X.-S., & Xiang, C.-Q. 2005, Phys. Plasmas, 11, 12
de Gouveia dal Pino, E., & Lazarian, A. 2005, A&A, 441, 845
Gruzinov, A. V., & Diamond, P. H. 1994, Phys. Rev. Lett., 72, 1651
Hanasz, M., Kowal, G., Otmianowska-Mazur, K., & Lesch, H. 2004, ApJ, 605, L33
Horbury, T. S., & Balogh, A. 2001, J. Geophys. Res., 106, 15929
Innes, D. E., Inhester, B., Axford, W. I., & Wilhelm, K. 1997, Nature, 386, 811
Kowal, G., Lazarian, A., Vishniac, E. T., & Otmianowska-Mazur, K. 2009, ApJ, 700, 63
Krause, F., & Radler, K. H. 1980, Mean-Field Magnetohydrodynamics and Dynamo Theory (Oxford: Pergamon Press)
Lazarian, A., & Opher, M. 2009, ApJ, 703, 8
Lazarian, A., & Vishniac, E. T. 1999, ApJ, 517, 700 (LV99)
Lazarian, A., & Vishniac, E. T. 2000, Rev. Mex. Astron. Astrofis., 9, 55
Lazarian, A., & Vishniac, E. T. 2008, in Rev. Mex. Astron. Astrofís. Conf. Ser., 36, 81
Lazarian, A., Vishniac, E., & Kowal, G. 2009, ASP Conf. Ser., 406, 23
Lesch, H. 1993, The Cosmic Dynamo, ed. F. Krause, Conf. Proc. IAU Symp., 157, 395
Londrillo, P., & Del Zanna, L. 2000, ApJ, 530, 508
Loureiro, L., Cowley, S. C., Dorland, W. D., Haines, M. G., & Schekochihin, P. 2005, Phys. Rev. Lett., 95, 235003
Loureiro, L., Uzdensky, N., Schekochihin, P., Cowley, S. C., & Yousef, T. A. 2009, MNRAS, 399, L146
Matthaeus, W. H., & Lamkin, S. L. 1985, Phys. Fluids, 28, 303
Matthaeus, W. H., & Lamkin, S. L. 1986, Phys. Fluids, 29, 2513
Matthaeus, W. H., Ambrosiano, J. J., & Goldstein, M. L. 1984, Phys. Rev. Lett., 53, 1449
McKee, C. F., & Ostriker, E. C. 2007, ARA&A, 45, 565
Mignone, A. 2007, J. Comput. Phys., 225, 1427
Moffat, H. K. 1978, Magnetic Field Generation in Electrically conducting Fluids (London, UK/New York, NY: Cambridge University Press)
Pagano, P., Raymond, J. C., Reale, F., & Orlando, S. 2008, A&A, 481, 835
Parker, E. N. 1957, J. Geophys. Res., 62, 509
Parker, E. N. 1979, Cosmical Magnetic Fields (Oxford, USA: Clarendon Press)
Parker, E. N. 1992, ApJ, 401, 137
Petschek, H. E. 1964, in Conf. Proc. AAS-NASA Symposium, Physics of Solar Flares, ed. W. H. Hess (Washington, DC: NASA Science and Technical Information Division), 425
Priest, E., & Forbes, T. 2000, Magnetic Reconnection (Cambridge, UK: Cambridge University Press)
Ruzmaikin A. A., Shukurov A. M., & Sokoloff D. D. 1988, Magnetic Fields of Galaxies, Ap&SS Library (Dordrecht: Kluwer Academic Publishers)
Santos-Lima, R., Lazarian, A., de Gouveia Dal Pino, E. M., & Cho, J. 2010, ApJ, 714, 442
Servidio, S., Matthaeus, W. H., Shay, M. H., Cassak, P. A., & Dmitruk, P. 2009, Phys. Rev. Lett., 101, 115003
Sweet, P. A. 1958, Electromagnetic Phenomena in Cosmical Physics, ed. B. Lehnert (Cambridge, UK:Cambridge University Press), Conf. Proc. IAU Symp., 6, 123
Tóth, G. 2000, JCoPh, 161, 605
Uzdensky, D. A. 2006, [arXiv:astro-ph/0607656]
Vainshtein, S. I., & Cattaneo, F. 1992, ApJ, 393, 165
Vishniac, E. T., & Lazarian, A. 1999, ApJ, 511, 193
Wu, C. C., & Chang, T. 2001, J. Atmos. Sol.-Terr. Phys., 63, 1447
Yamada, M., Ren, Y., Ji, H., et al. 2006, Phys. Plasmas, 13, 052119
Yokoyama, T., & Shibata, K. 1995, Nature, 375, 42